Using higher ionization states to increase Coulomb coupling in an ultracold neutral plasma

M. Lyon, S. D. Bergeson, A. Diaw, and M. S. Murillo

Phys. Rev. E **91**, 033101 — Published 2 March 2015

DOI: 10.1103/PhysRevE.91.033101

Using higher ionization states to increase Coulomb coupling in an ultracold neutral plasma

M. Lyon,[1,*] S. D. Bergeson,[1] A. Diaw,[2] and M. S. Murillo[2]

[1] *Department of Physics and Astronomy, Brigham Young University, Provo, UT 84602, USA*
[2] *New Mexico Consortium, Los Alamos, New Mexico 87544*

(Dated: February 6, 2015)

We report measurements and simulations of the time-evolving rms velocity distribution in an ultracold neutral plasma. A strongly coupled ultracold neutral Ca^+ plasma is generated by photoionizing laser-cooled atoms close to threshold. A fraction of these ions are then promoted to the second ionization state to form a mixed Ca^+/Ca^{2+} plasma. By varying the time delay between first and second ionization events, a minimum in ion heating is achieved. We show that the Coulomb strong coupling parameter Γ increases by a factor of 1.4 to a maximum value of 3.6. A pure Ca^{2+} plasma would have $\Gamma = 6.8$, moving these strongly-coupled systems closer to the regime of liquid-like correlations.

PACS numbers: 52.27.Gr, 52.20.-j, 79.70.+q, 52.25.Jm

Plasmas comprise the vast majority of the known universe and exist over a wide range of temperatures and densities. At sufficiently high densities, certain astrophysical systems such as the interior of some Jovian planets and white dwarf stars and the outer crust of neutron stars form strongly coupled plasmas. Strong coupling is also a property of a number of dusty and laser-produced plasmas, which include high energy-density fusion plasmas at one extreme [1–5], and low temperature, low density, ultracold neutral plasmas at the other extreme [6–27].

Many plasma properties scale with the dimensionless coupling parameter $\Gamma = (Z^2e^2/4\pi\epsilon_0 a_{\rm ws})(1/k_{\rm B}T_{\rm i})$, where Z is the ion charge state, e is the fundamental charge, $a_{\rm ws} \equiv (3/4\pi n)^{1/3}$ is the Wigner-Seitz radius, n is the plasma density, $k_{\rm B}$ is Boltzman's constant, and $T_{\rm i}$ is the ion temperature. This parameter, called the strong Coulomb coupling parameter, is given by the ratio of the nearest-neighbor electrical potential energy to the average ion kinetic energy. Strongly coupled systems can differ by orders of magnitude in temperature and density. However Γ-scaling shows that they share many of the same characteristics, thus making it possible to study strongly coupled high energy-density plasmas as well as liquid-like systems at very low energy [28–30].

The value of Γ in ultracold neutral plasmas is typically limited to $\Gamma = 2.5$, although higher values may be achievable [23]. This limit is a result of the an ultrafast, non-equilibrium relaxation of the ions due to spatial disorder in the system [7, 31, 32]. The locations of the neutral atoms before ionization are spatially uncorrelated. When the atoms are ionized, each ion finds itself in a potential defined primarily by Coulomb interactions with neighboring charged particles. Ions move from a disordered state (high potential energy) to a more ordered state (low potential energy), increasing their kinetic energy and heating the plasma. This heating mechanism is called "disorder-induced heating" (DIH), and the initially $T \sim$ mK ions heat to the correlation temperature $T_{\rm c} = (2/3)(e^2/4\pi\epsilon_0 a_{\rm ws}k_{\rm B})$ [31] on the time scale of the inverse ion plasma frequency, $1/\omega_{\rm p,i} = (ne^2/m_{\rm i}\epsilon_0)^{-1/2}$, where $m_{\rm i}$ is the ion mass.

Overcoming the DIH limitation would make it possible for these ultracold neutral plasmas to move into the liquid-like correlation regime [33–37]. Energy relaxation, wave damping, collisional transport and diffusion for neutral plasmas are not well understood under these conditions, in spite of their importance for warm dense matter [38, 39]. Strongly-coupled plasmas are predicted to have enhanced collision rates leading to enhanced thermonuclear fusion rates [40]. However, this enhancement has only been seen in laser-cooled one-component plasma experiments [41–43] – never in a neutral system.

Earlier work in ultracold neutral plasmas suggested that the strong-coupling parameter might be as high as 4 [11, 44]. However, recent work has highlighted the role of electron screening in reducing the coupling constant to values near 2.5 or less [7]. The role of screening in strongly-coupled systems is an ongoing research topic [45], and no universal explanation of strong coupling in screened systems exists.

In this paper, we describe a new experiment that can overcome the limit of $\Gamma = 2.5$ imposed by disorder-induced heating [7]. This makes is possible to extend collision studies farther into the strongly coupled regime [28]. Although the experimentally realized gains in this paper are modest, our simulations show that this method can be used to reach $\Gamma = 6.8$. One other paper reports a neutral plasma in which the strong coupling parameter is probably higher [23], and there are proposals for other ways of increasing Γ [46–48]. However, the present work reports the highest value of Γ in a neutral system in which optical diagnostics are possible.

The initial ion motion due to DIH is coherent. The ions start moving all at the same time, and the average kinetic energy oscillates. A recent simulation predicted

this quasi-coherent kinetic energy oscillation could be exploited to achieve higher values of the strong coupling parameter [49]. When the ions first reach their maximum kinetic energy, they could be promoted to the second ionization state. The simulation showed that second-ionization at this particular time generated minimal heating of the ions while quadrupling the nearest-neighbor Coulomb potential energy.

In this Letter we report measurements and simulations of the rms velocity distribution in a mixed Ca^+/Ca^{2+} plasma. Laser-cooled calcium atoms in a MOT are first resonantly ionized to form a Ca^+ plasma. At a variable time after this initial ionization event, a portion of the Ca^+ ions are ionized to Ca^{2+}. By varying the time delay between the first and second ionization events, we show that a minimum in ion heating is achieved. We simulate the rms ion velocity distribution in this mixed plasma and extract the average electrical potential energy. We show that the Coulomb strong coupling parameter, Γ, increases by a factor of 1.4, from an initial value of 2.5 to a maximum value of 3.6 in our experiment. The simulations indicate that a pure Ca^{2+} plasma would have $\Gamma = 6.8$.

Approximately 20 million ^{40}Ca atoms are trapped in a magneto-optical trap, with a Gaussian spatial density profile of the form $n(r) = n_0 \exp(-r^2/2\sigma^2)$, with peak density $n_0 \leq 3.5 \times 10^{10}$ cm^{-3} and $\sigma = 0.3$ mm. We photoionize the atoms in a two photon ionization process using 7 ns pulses at 423 and 390 nm that drive the $4s^2\ ^1S_0 \rightarrow 4s4p\ ^1P_1^o$ and the $4s4p\ ^1P_1^o \rightarrow$ continuum transitions, respectively. The initial electron energy is set by the wavelength of the ionizing laser, because the excess photon energy above the ionization limit is carried away by the electrons. The density and first ionization fraction are measured using absorption techniques. For this work, close to 100% of the atoms in the MOT are converted into Ca^+. The wavelength of the 390 nm ionizing laser is set above threshold so that the initial electron temperature is approximately $T_e = 2E_e/3k_B \approx\sim$ 190 K. This greatly reduces three-body recombination [14], which has the potential to adversely influence our measurements.

We use additional pulsed lasers to generate the Ca^{2+} plasma. The excitation pathway uses the $4s\ ^2S_{1/2} \rightarrow 4p\ ^2P_{1/2}^o$ transition at 397 nm, the $4p\ ^2P_{1/2}^o \rightarrow 5d\ ^2D_{3/2}$ transition at 210 nm, and finally the $5d\ ^2D_{3/2} \rightarrow$ continuum transition (see inset to Fig. 1). The bound-bound transitions are driven by frequency doubling or quadrupling pulse-amplified cw lasers. The last step into the continuum requires much more power, and we use the third harmonic of a pulsed ND:YAG laser at 355 nm. The 355 nm pulse can be attenuated using a polarizer and a beam splitter. Varying the 355 nm pulse energy allows us to change the second ionization fraction, which ranges from 10-30%. We use an acousto-optical modulator (AOM) to turn off the MOT beams about 12 μs before the first ionization so that the 355 nm pulse does not ionize excited state neutral atoms in the MOT. These neutral atoms can come from atoms that were not ionized with the 390 nm pulse, or from recombined ions.

We probe the velocity distribution of the remaining Ca^+ ions using laser-induced fluorescence [11]. Approximately 1 W at 794 nm from a tunable cw Ti:sapphire laser is frequency doubled to 397 nm, which corresponds to the $4s\ ^2S_{1/2} \rightarrow 4p\ ^2P_{1/2}^o$ transition in Ca^+. The frequency is fixed by locking the laser to a partially stabilized frequency comb in the fundamental, as described in Ref. [50]. The doubled light is then collimated to a diameter of 6 mm, attenuated to 2 mW, aligned to spatially overlap plasma, and retroreflected. We scan the probe laser frequency across the interval $\pm$200 MHz from line center [50]. Fluorescence at 397 nm is collected as a function of time using a 1-GHz bandwidth photo-multiplier tube and digital oscilloscope.

To extract the time evolving ion velocity $v_{\rm i,rms}$, we fit the fluorescence data to a Voigt profile [7]. The Lorentzian contribution is given by the 22 MHz natural linewidth of the transition. The measured linewidth is Doppler broadened as the plasma ions accelerate. The Gaussian width is extracted as a fit parameter and is connected to the velocity of the ions through the Doppler shift $v_{\rm i,rms} = (k_{\rm B}T_{\rm i}/m_{\rm i})^{1/2} = \lambda\nu_{\rm rms}$, allowing us to map out the width of the ion velocity distribution as a function of time, as shown in Fig. 1. Comparing the integrated Voigt profile, before and after the second ionization step, gives us an estimate the second ionization fraction.

The ion temperature evolves in time, due to DIH and the plasma expansion. The rms ion velocity $v_{\rm i,rms}$ is related to the ion and electron temperatures as [18]

$$v_{\rm i,rms} = \sqrt{\frac{k_B}{m_{\rm i}}\left\{\frac{t^2}{\tau_{\rm exp}^2}[T_{\rm e}(t) + T_{\rm i}(t)] + T_{\rm i}(t)\right\}}, \quad (1)$$

where the characteristic expansion time $\tau_{\rm exp}$ is given by $\tau_{\rm exp} = \sqrt{m_{\rm i}\sigma(0)^2/k_{\rm B}[T_{\rm e}(0) + T_{\rm i}(0)]}$ and the ion and electron temperatures are given by $T_{\rm i,e}(t) = T_{\rm i,e}(0)/(1 + t^2/\tau_{\rm exp}^2)$. Figure 1 shows the experimental $v_{\rm i,rms}$ for a singly ionized plasma (lower curve). The dashed line shows the model of Eq. 1.

After a time delay, $0 \leq t \leq 300$ ns, a fraction of the Ca^+ ions are converted to Ca^{2+}. This change in the ion density results in an additional DIH phase as the combined ion system equilibrates again. The resulting ion velocity distribution is comprised of contributions from the original ion system as well as that of the Ca^{2+} system. We isolate the additional contribution to the ion velocity that arises from the second ionization by subtracting off (in quadrature) the expansion of the original Ca^+ system that we obtain from the model (black dashed line in Fig. 1). For the purposes of extracting the increased ion temperature, we identify the time at which the second ionization laser pulses arrive as the new "zero" of time.

We use the expansion model described by Eq. 1 and fit it to the data (with the Ca^+ model subtracted) to find the increase in the ion and electron temperatures. The new T_i calculated in this way is the additional heating from the second ionization, ΔT_i. In this mixed Ca^+/Ca^{2+} plasma, the electron temperature increases typically to 600 K due to the 355 nm ionizing laser. The combined expansion model is plotted with the measured rms ion velocity as the upper data and dashed line in Fig. 1.

We simulate the experiments using molecular dynamics (MD) [49]. In the simulations, the ions interact via the Yukawa potential,

$$u_Y(r) = \frac{Ze}{4\pi\epsilon_0}\frac{\exp(-\kappa r_{ij})}{r_{ij}}, \tag{2}$$

where $\kappa = a_{ws}/\lambda_D$ is the inverse scaled screening length, $\lambda_D = (k_B T_e \epsilon_0/ne^2)^{1/2}$ is the Debye length, and $Z = 1, 2$ is the ionization state. We initially place Yukawa particles with $Z = 1$ randomly in the main simulation cell with an average density measured in the experiment. The equations of motion of the N particles are integrated using a second-order symplectic integrator (velocity-Verlet) subject to periodic boundary conditions. To check for finite-size effects in our simulation, we vary the number of particles up to $N = 10,000$ and find that $N \sim 6000$ is sufficient.

To simulate the second ionization event, we randomly replace a fraction of the $Z = 1$ ions with $Z = 2$ ions at a given time delay. In the experiment, this fraction maximizes at approximately 30%, a limit evidently set by competition between optical pumping and ionization rates in the $Ca^+ \rightarrow Ca^{2+}$ process. The electron screening length is adjusted by the increase in electron temperature and density using the conditions used in the experiment. The simulation then continues in this mixed Ca^+/Ca^{2+} state. From the simulated ion trajectories, we calculate the effective temperature (second-moment of the velocity distribution) using

$$T(t) = \frac{m}{3Nk_B}\sum_{j=1}^{N}\left\langle v_j^2(t)\right\rangle, \tag{3}$$

where N is the total number of ions in the simulation. Although in a non-equilibrium plasma configuration "temperature" is not strictly defined, this average mean-squared velocity corresponds directly to experimental measurements. Simulation results are summarized in Fig. 2.

In Fig. 3, we compare the experimentally determined change in the ion temperature with the results of the MD simulation. The change in the ion temperature is minimized near $\omega_p t \sim 2$, where the first kinetic energy oscillation peak occurs. The uncertainty in the experimental measurements is shown by the error bars. The largest error is associated with statistical uncertainties in extracting the increased rms ion velocity. Because our line-shape spectroscopy and Ca^{2+} ionization pathways use the same atomic transitions, scattered light and optical pumping prevents analysis of data closer than 50 ns after the second set of laser pulses. This limits our analysis to expansion data that is dominated by the electron temperature, leading to somewhat larger uncertainties in determining ΔT_i from the second ionization. Laser power jitter strongly influences the electron temperature. There is an additional source of error due to the relative timing of the laser pulses, which can drift by several ns during the experiment. However, the experiment shows the achievement of additional ionization with minimal heating of the plasma.

The Coulomb coupling was computed from the MD simulation using

$$\Gamma = \frac{\langle Z^{5/3}\rangle\langle Z^{1/3}\rangle e^2}{4\pi\epsilon_0 a_{ws} k_B T_i(t)}, \tag{4}$$

where $T_i(t)$ is the time-evolving ion temperature and the moments $\langle Z^\alpha\rangle$ account for the Ca^+/Ca^{2+} mixture. Computing the potential energy in the naively more straightforward way, for example, $\langle U\rangle = \frac{1}{N^2}\sum_i^N\sum_{j\neq i}^N (Z_i Z_j e^2)/(4\pi\epsilon_0 r_{ij})$, leaves out important contributions from electron-electron and electron-ion interactions (detailed screening among the components, cloud-cloud interactions, etc.) which are critical in determining the electrical potential energy of the system [7]. The calculated value of Γ, which is the ratio of the potential energy to the temperature, is shown in Fig. 2. For an ionization fraction of 20%, Γ increases from 2.5 to 3.6. Our simulations show that increasing the ionization fraction to 100% would increase the strong coupling parameter to $\Gamma = 6.8$ (see Fig. 2d).

In conclusion, we report measurements and simulations of the rms ion velocity in a mixed $Ca+/Ca^{2+}$ plasma. We show that the ion temperature depends on the time delay between the first and second ionization events. In this work, we demonstrate an increase in the strong coupling parameter from $\Gamma = 2.5$ to $\Gamma = 3.6$. We show that $\Gamma = 6.8$ is possible with increased ionization efficiency.

This work opens a new window of opportunity for generating strongly coupled plasmas. Successive excitation to even higher ionization states would increase Γ by nearly Z^2 compared to the singly-ionized plasma. Most of the ultracold neutral plasma experiments are limited to the regime of $\Gamma \approx 2$ because of the DIH process. A number of important and interesting studies are focused on overcoming this limitation. We have previously shown that electron shielding decreases the ion temperature [7]. Gradual heating of the electrons in a strongly shielded plasma could increase Γ to approximately 4. Using the Rydberg blockade to enhance spatial order before ionization could lead to Γ in the range of 10 to 30 [46] and work along these lines is in progress [47]. Recent work in an ultracold molecular plasma suggests that $\Gamma = 50$ may be

possible [23]. Cooling by adiabatic plasma expansion is another possible pathway to more strongly coupled plasmas [48]. Finally, we mention the possibility of laser-cooling the ions, which is underway in our lab. When these efforts are successful, the field of strongly coupled plasmas will have new exciting opportunities for studying neutral plasma dynamics in a novel portion of phase space.

ACKNOWLEDGMENTS

This work is supported in part by the National Science Foundation (grant no PHY-0969856) and the Air Force (grant no. FA9950-12-1-0308). M. Lyon recognizes funding from the Utah NASA Space Grant Consortium.

* mary_lyon@byu.edu

[1] H.-S. Park, *et al.* Phys. Rev. Lett. **112**, 055001 (2014).
[2] M. J. Edwards and *et. al.*, Physics of Plasmas **18**, 051003 (2011).
[3] M. J. Edwards and *et. al.*, Physics of Plasmas (1994-present) **20**, 070501 (2013).
[4] J. L. Kline,*et al.*Phys. Rev. Lett. **106**, 085003 (2011).
[5] N. B. Meezan, *et al.*Physics of Plasmas **17**, 056304 (2010).
[6] M. S. Murillo, Journal of Physics A: Mathematical and Theoretical **42**, 214054 (2009).
[7] M. Lyon, S. D. Bergeson, and M. S. Murillo, Phys. Rev. E **87**, 033101 (2013).
[8] M. Lyon and S. D. Bergeson, Journal of Physics B: Atomic, Molecular and Optical Physics **44**, 184014 (2011).
[9] S. D. Bergeson, A. Denning, M. Lyon, and F. Robicheaux, Phys. Rev. A **83**, 023409 (2011).
[10] M. S. Murillo, Phys. Rev. Lett. **87**, 115003 (2001).
[11] E. A. Cummings, J. E. Daily, D. S. Durfee, and S. D. Bergeson, Phys. Rev. Lett. **95**, 235001 (2005).
[12] T. C. Killian, M. J. Lim, S. Kulin, R. Dumke, S. D. Bergeson, and S. L. Rolston, Phys. Rev. Lett. **86**, 3759 (2001).
[13] R. S. Fletcher, X. L. Zhang, and S. L. Rolston, Phys. Rev. Lett. **99**, 145001 (2007).
[14] S. D. Bergeson and F. Robicheaux, Phys. Rev. Lett. **101**, 073202 (2008).
[15] J. Castro, P. McQuillen, and T. C. Killian, Phys. Rev. Lett. **105**, 065004 (2010).
[16] T. C. Killian, P. McQuillen, T. M. O'Neil, and J. Castro, Physics of Plasmas (1994-present) **19**, 055701 (2012).
[17] S. Kulin, T. C. Killian, S. D. Bergeson, and S. L. Rolston, Phys. Rev. Lett. **85**, 318 (2000).
[18] S. Laha, P. Gupta, C. E. Simien, H. Gao, J. Castro, T. Pohl, and T. C. Killian, Physical Review Letters **99**, 155001 (2007).
[19] R. S. Fletcher, X. L. Zhang, and S. L. Rolston, **96**, 105003 (2007).
[20] K. A. Twedt and S. L. Rolston, Phys. Rev. Lett. **108**, 065003 (2012).
[21] T. Pohl, T. Pattard, and J. M. Rost, Phys. Rev. A **70**, 033416 (2004).
[22] S. Laha, Y. C. Chen, P. Gupta, C. E. Simien, Y. N. Martinez, P. G. Mickelson, S. B. Nagel, and T. C. Killian, Eur. Phys. J. D , 51 (2006).
[23] H. Sadeghi, A. Kruyen, J. Hung, J. H. Gurian, J. P. Morrison, M. Schulz-Weiling, N. Saquet, C. J. Rennick, and E. R. Grant, Phys. Rev. Lett. **112**, 075001 (2014).
[24] M. Siercke, F. E. Oon, A. Mohan, Z. W. Wang, M. J. Lim, and R. Dumke, Phys. Rev. A **89**, 022701 (2014).
[25] F. Robicheaux, M. M. Goforth, and M. A. Phillips, Phys. Rev. A **90**, 022712 (2014).
[26] J. Hung, H. Sadeghi, M. Schulz-Weiling, and E. R. Grant, Journal of Physics B: Atomic, Molecular and Optical Physics **47**, 155301 (2014).
[27] C. Witte and J. Roberts, "Ultracold plasma expansion as a function of charge neutrality," arXiv:1409.1611 (2014).
[28] G. Bannasch, J. Castro, P. McQuillen, T. Pohl, and T. C. Killian, Phys. Rev. Lett. **109**, 185008 (2012).
[29] S. D. Baalrud and J. Daligault, Phys. Rev. Lett. **110**, 235001 (2013).
[30] S. L. Rolston, Physics **1**, 2 (2008).
[31] Y. C. Chen, C. E. Simien, S. Laha, P. Gupta, Y. N. Martinez, P. G. Mickelson, S. B. Nagel, and T. C. Killian, Phys. Rev. Lett. **93**, 265003 (2004).
[32] M. S. Murillo, Phys. Rev. Lett. **96**, 165001 (2006).
[33] B. Tata, P. Rajamani, J. Chakrabarti, A. Nikolov, and D. Wasan, Phys. Rev. Lett. **84**, 3626 (2000).
[34] N. Clark and D. Coleman, Phys. Rev. Lett. **87**, 029601 (2001).
[35] J. Lischner and T. Arias, Phys. Rev. Lett. **101**, 216401 (2008).
[36] J. King, M. Ross, and K. Kubarych, Phys. Rev. Lett. **108**, 157401 (2012).
[37] G. Biroli, C. Cammarota, G. Tarjus, and M. Tarzia, Phys. Rev. Lett. **112**, 175701 (2014).
[38] V. Fortov, R. Ilkaev, V. Arinin, V. Burtzev, V. Golubev, I. Iosilevskiy, V. Khrustalev, A. Mikhailov, M. Mochalov, V. Ternovoi, and M. Zhernokletov, Phys. Rev. Lett. **99**, 185001 (2007).
[39] C. R. D. Brown and *et. al.*, Scientific Reports **4** (2014), http://dx.doi.org/10.1038/srep05214.
[40] E. E. Salpeter and H. M. V. Horn, Astrophys. J. **155**, 183 (1969).
[41] M. J. Jensen, T. Hasegawa, J. J. Bollinger, and D. H. E. Dubin, Phys. Rev. Lett. **94**, 025001 (2005).
[42] D. H. E. Dubin, Phys. Rev. Lett. **94**, 025002 (2005).
[43] F. Anderegg, D. H. E. Dubin, T. M. O'Neil, and C. F. Driscoll, Phys. Rev. Lett. **102**, 185001 (2009).
[44] C. E. Simien, Y. C. Chen, P. Gupta, S. Laha, Y. N. Martinez, P. G. Mickelson, S. B. Nagel, and T. C. Killian, Phys. Rev. Lett. **92**, 143001 (2004).
[45] T. Ott, M. Bonitz, L. G. Stanton, and M. S. Murillo, Physics of Plasmas (1994-present) **21**, 113704 (2014).
[46] G. Bannasch, T. C. Killian, and T. Pohl, Phys. Rev. Lett. **110**, 253003 (2013).
[47] P. McQuillen, X. Zhang, T. Strickler, F. B. Dunning, and T. C. Killian, Phys. Rev. A **87**, 013407 (2013).
[48] P. McQuillen, T. Langin, T. Strickler, and T. Killian, Bull. Am. Phys. Soc. **59** (2014).
[49] M. S. Murillo, Physics of Plasmas **14**, 055702 (2007).
[50] M. Lyon and S. D. Bergeson, Appl. Opt. **53**, 5163 (2014).

FIGURES

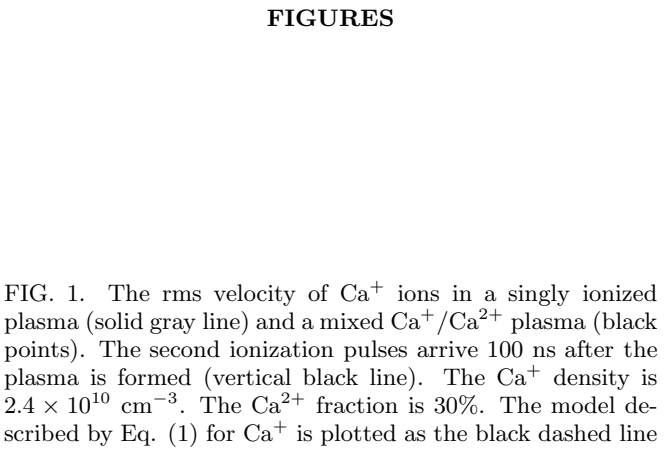

FIG. 1. The rms velocity of Ca^+ ions in a singly ionized plasma (solid gray line) and a mixed Ca^+/Ca^{2+} plasma (black points). The second ionization pulses arrive 100 ns after the plasma is formed (vertical black line). The Ca^+ density is 2.4×10^{10} cm^{-3}. The Ca^{2+} fraction is 30%. The model described by Eq. (1) for Ca^+ is plotted as the black dashed line and for Ca2+ is plotted as the gray dasned line (see text). **Inset:** Partial energy level diagram for Ca (left) and Ca^+ (right). Neutral Ca atoms are trapped using the 423 nm transition. The Ca^+ ions are created using laser pulses at 423 nm and 390 nm. Laser-induced fluorescence measurements are made using a cw probe laser tuned to the 397 nm transition. The Ca^{2+} ions are created using laser pulses at 397 nm, 210 nm, and 355 nm.

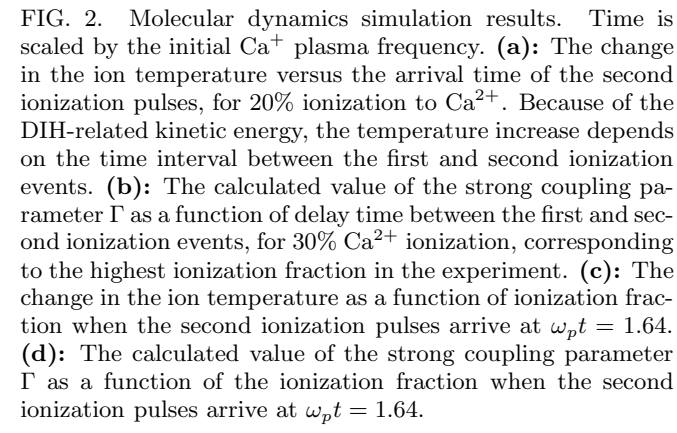

FIG. 2. Molecular dynamics simulation results. Time is scaled by the initial Ca^+ plasma frequency. **(a):** The change in the ion temperature versus the arrival time of the second ionization pulses, for 20% ionization to Ca^{2+}. Because of the DIH-related kinetic energy, the temperature increase depends on the time interval between the first and second ionization events. **(b):** The calculated value of the strong coupling parameter Γ as a function of delay time between the first and second ionization events, for 30% Ca^{2+} ionization, corresponding to the highest ionization fraction in the experiment. **(c):** The change in the ion temperature as a function of ionization fraction when the second ionization pulses arrive at $\omega_p t = 1.64$. **(d):** The calculated value of the strong coupling parameter Γ as a function of the ionization fraction when the second ionization pulses arrive at $\omega_p t = 1.64$.

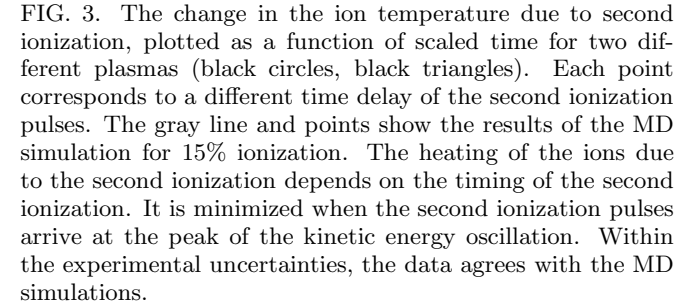

FIG. 3. The change in the ion temperature due to second ionization, plotted as a function of scaled time for two different plasmas (black circles, black triangles). Each point corresponds to a different time delay of the second ionization pulses. The gray line and points show the results of the MD simulation for 15% ionization. The heating of the ions due to the second ionization depends on the timing of the second ionization. It is minimized when the second ionization pulses arrive at the peak of the kinetic energy oscillation. Within the experimental uncertainties, the data agrees with the MD simulations.

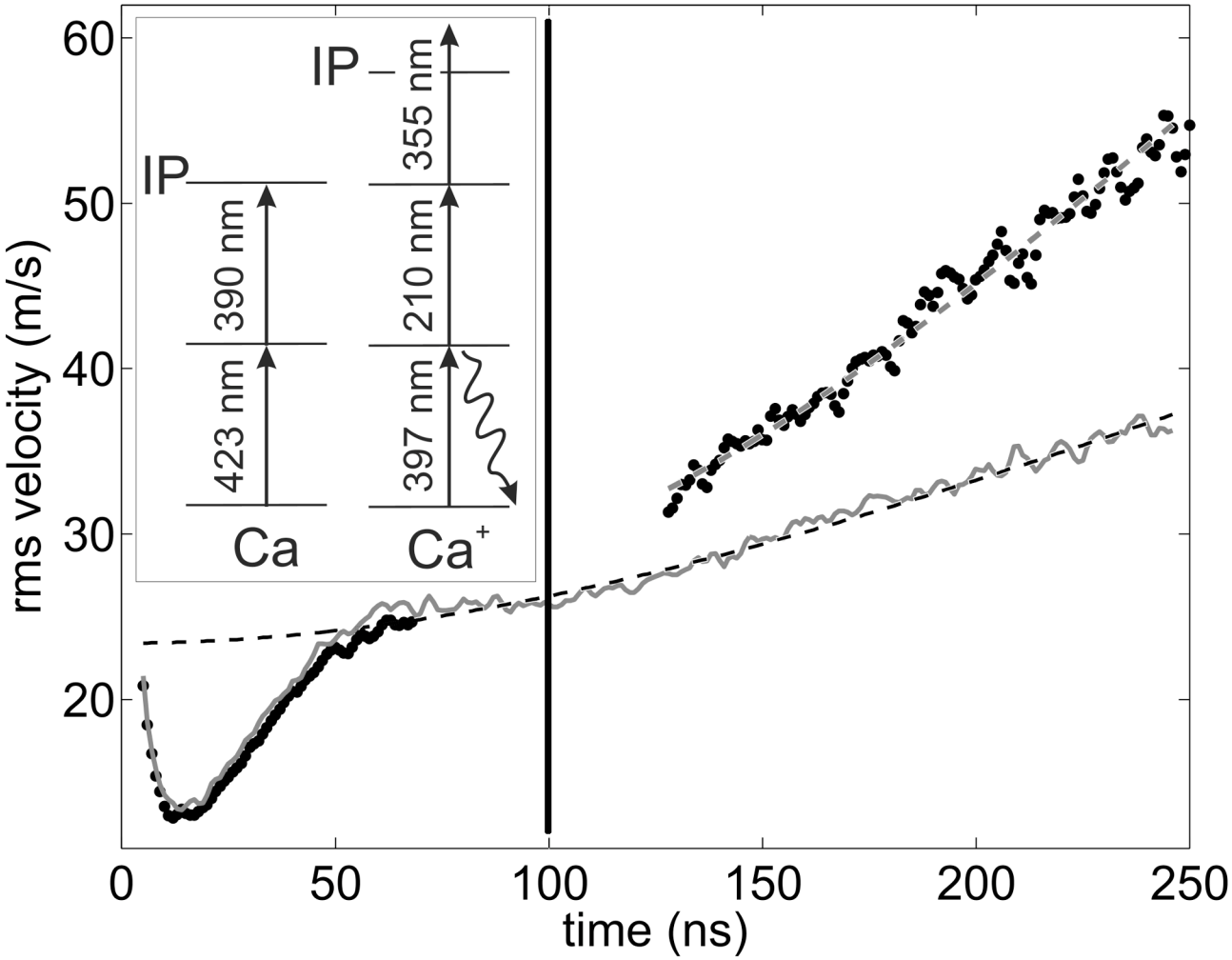

Figure 1 06Feb2015

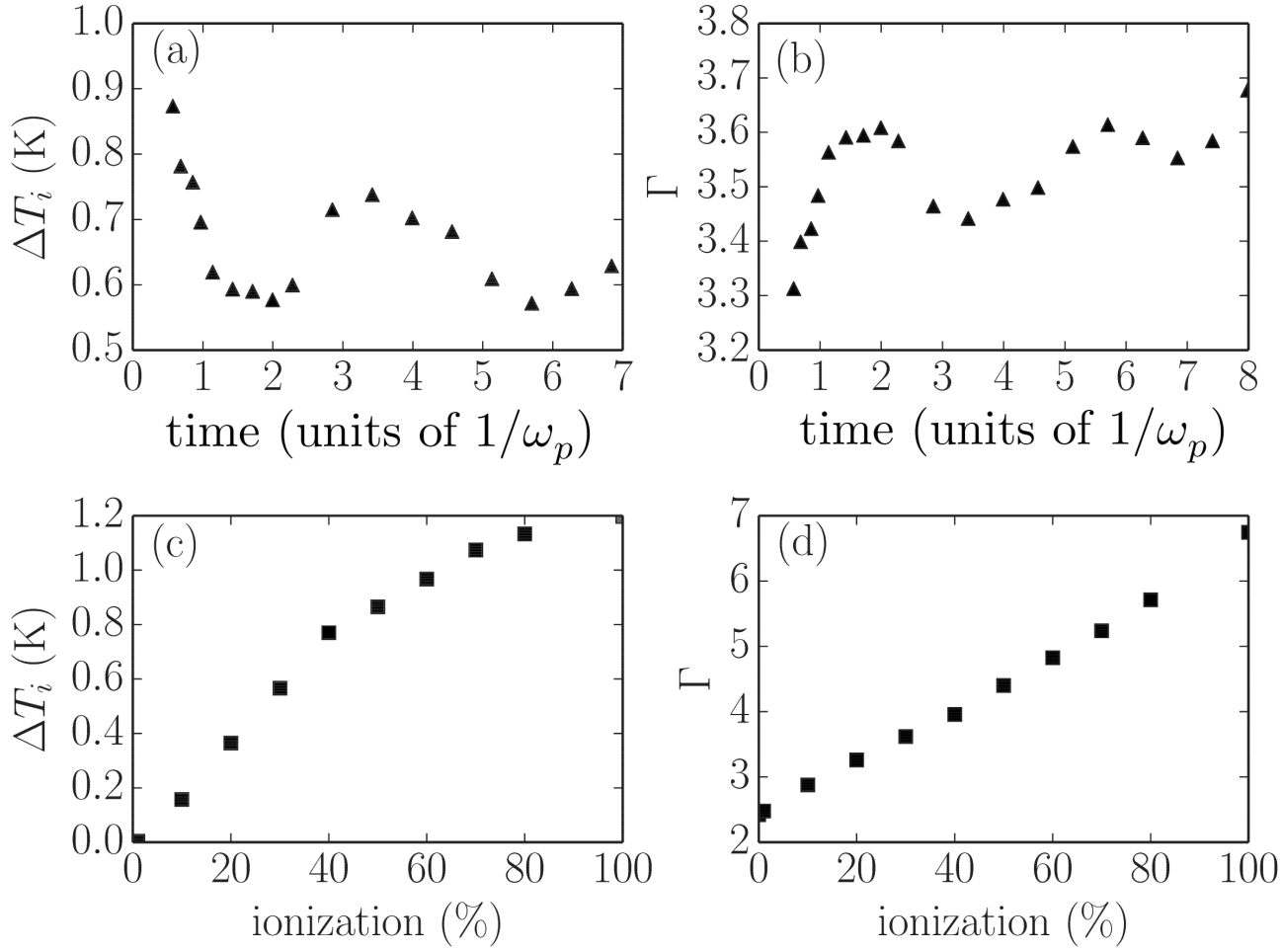

Figure 2 06Feb2015

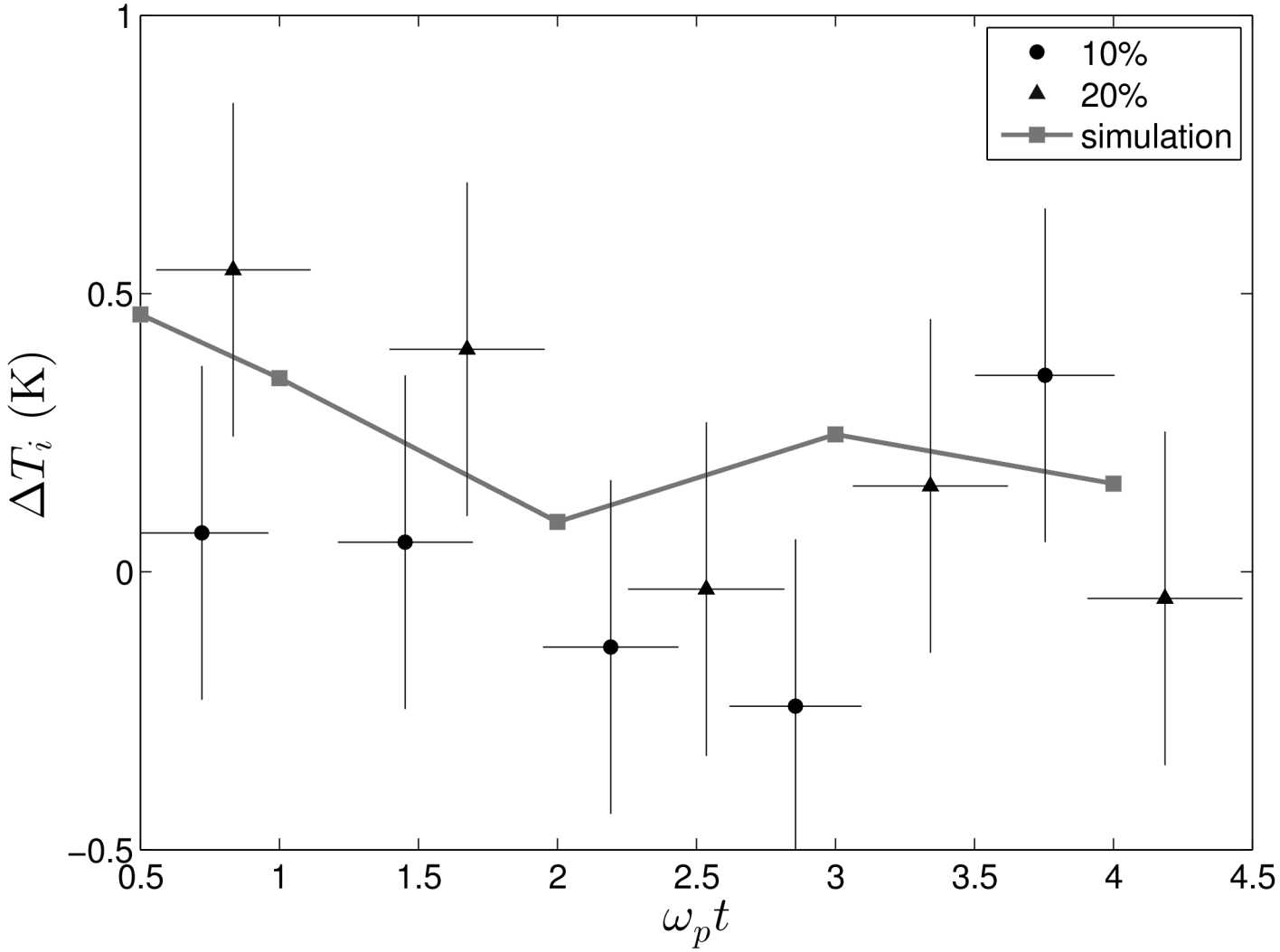

Figure 3 06Feb2015